Capturing cyclic mobility and preloading effects in sand using a memory-surface hardening model

Liu, Haoyuan; Abell, J. A.; Diambra, A.; Pisano, Federico

Publication date
2019

Document Version
Accepted author manuscript

Published in
Earthquake Geotechnical Engineering for Protection and Development of Environment and Constructions

Capturing cyclic mobility and preloading effects in sand using a memory-surface hardening model

H.Y. Liu
Faculty of Civil Engineering and Geosciences, Delft University of Technology, Delft, The Netherlands

J.A. Abell
Facultad de Ingeniera y Ciencias Aplicadas, Universidad de los Andes, Santiago, Chile

A. Diambra
Department of Civil Engineering, Faculty of Engineering, University of Bristol, Bristol, UK

F. Pisanò
Faculty of Civil Engineering and Geosciences, Delft University of Technology, Delft, The Netherlands

ABSTRACT: Earthquake-induced build-up of pore water pressure may be responsible for reduced soil capacity, while the accumulation of shear strains may lead to a violation of serviceability limits. Predicting accurately the soil cyclic behaviour in relation to seismic numerical simulations is still a challenging topic in many respects. Efforts are required to improve several technical aspects, including the development of a reliable and complete constitutive model. This paper reports recent developments after the work of Liu et al. (2018a), and particularly about the performance of a new SANISAND formulation incorporating the memory surface concept (Corti et al., 2016). The performance of the model in terms of strain accumulation and pore pressure build-up is validated against high-quality laboratory test results. A modified dilatancy relationship is given to reproduce within the proposed framework proper cyclic mobility response. The effects of preliminary drained cyclic preloading on soil liquefaction resistance are also studied.

1 INTRODUCTION

During earthquakes, the generation of excess pore water pressure under undrained dynamic loading conditions decreases the soil bearing capacity and/or may cause serviceability issues in geotechnical systems (Andersen, 2009). Under undrained cyclic loadings, granular soils (e.g. sands) experience different failure modes, depending on the sand properties and loading conditions (Elgamal et al., 2003; Yang and Sze, 2011; Ziotopoulou and Boulanger, 2013): (1) flow liquefaction, consisting of a sudden pore water pressure build-up and runaway deformation, usually occurs on very loose sand; (2) cyclic mobility generally occurs for dense or medium dense sands which may exhibit repeated cycles of pore water pressure dissipation and regeneration after a transient initial liquefaction (Ishihara, 1993); or (3) excessive plastic strain accumulation which may occur under asymmetric loading conditions.

Accurate prediction of the undrained cyclic behaviour of the sands, which received serious attention in the past several decades, still calls for more reliable constitutive laws able to fully predict the complex soil response from small to large strains. In this context, most sand constitutive models for earthquake geotechnics can only qualitatively capture sand undrained cyclic behaviour or employ over-complex constitutive relations to ensure accurate quantitative prediction.

Recently, Liu et al. (2018a) combined the SANISAND04 (Dafalias and Manzari, 2004) with the hardening memory surface concept proposed by Corti et al. (2016). In this model, the soil fabric and its influence are phenomenologically represented by the newly introduced memory surface. The model features a fully multi-axial formulation, and has been proven to be effective in simulating sand ratcheting behaviour under high-cyclic loading conditions (Liu et al., 2018a,b; Liu and

Pisanò, 2018). Besides, the recent preliminary developments by Liu et al. (2018a) have extended the model capabilities to the simulation of undrained cyclic response of sand. The enhanced model is able to accurately predict the generation of pore water pressure at given loading cycles before initial liquefaction occurs. However, the model performance in reproducing the full soil stress-strain relationship, especially during the cyclic mobility stage, still requires improvements. Furthermore, its capacity of simulating cyclic preloading effects is to be further explored.

This paper aims to fill this gap and to develop an enhanced memory-surface model which would permit the real time-domain simulation of short loading events in numerical simulations. Starring from the memory-enhanced bounding surface model (Liu et al., 2018a), more robust flow rule and memory surface evolution law are proposed to create a model effective in predicting the pore water pressure generation in sand under cyclic undrained loading conditions. Emphasis is directed to accurately reproduce the full undrained stress-strain loop of cyclic mobility. The proposed model is validated by comparing the simulation results with undrained cyclic triaxial test results provided by Wichtmann (2005). The different soil responses under symmetric cyclic loading pattern with and without cyclic preloading are studied.

2 MODEL FORMULATION

In this section, the main features of the memory-enhanced SANISAND model by Liu et al. (2018a) is recalled. Detailed model formulation refers to the original publication. Meanwhile, the new flow rule and the memory surface evolution law are given.

The model embeds the hardening memory surface concept (Corti et al., 2016) into the parent SANISAND04 (Dafalias and Manzari, 2004) framework. The outcome is a three-surface (bounding, yield and memory surface) model, which links the critical state theory with the state parameter concept (Been and Jefferies, 1985). The model is defined directly in the normalised stress ratio π plane, as shown in Figure 1a. The memory surface is implemented to phenomenologically

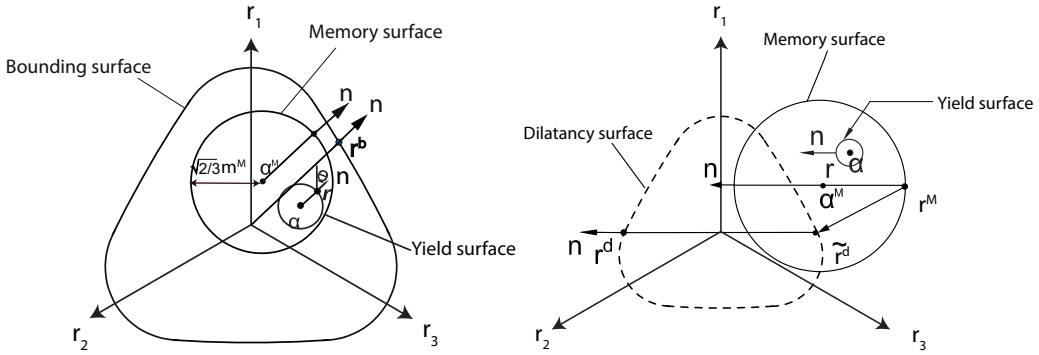

(a) Model surfaces, stress ratios and directions. (b) Representation of dilatancy mechanisms.

Figure 1.: The memory-enhanced bounding surface model by Liu et al. (2018a).

reflect the evolution and influence of soil fabric. The evolution of the memory surface obeys two basic rules: (1) the evolution of the memory surface is linked to the soil plastic deformation; (2) the memory surface always encloses the current yield surface and the current stress state. The impact of the memory surface on the soil stiffness is introduced by treating it as an additional reference surface. As such, the hardening modulus K_p is not only determined by the distance between current stress ratio $\boldsymbol{r}$ and its image point on the bounding surface $\boldsymbol{r}^b$, but also by the term $b^M = (\boldsymbol{r}^M - \boldsymbol{r}) : \boldsymbol{n}$, which indicates the distance between the current stress ratio point $\boldsymbol{r}$ and its projection on the memory surface $\boldsymbol{r}^M$, see Equation (1):

$$K_p = \frac{2}{3} p h (\mathbf{r}^b - \mathbf{r}) : \mathbf{n} \quad \text{with} \quad h = \frac{b_0}{(\mathbf{r} - \mathbf{r}_{in}) : \mathbf{n}} \exp\left[\mu_0 \left(\frac{p}{p_{atm}}\right)^{0.5} \left(\frac{b^M}{b_{ref}}\right)^2\right] \tag{1}$$

where μ_0 is a memory surface parameter quantifying the fabric impact on soil stiffness especially during cyclic loading. A pressure-dependent term $(p/p_{atm})^{0.5}$ is included to improve model prediction over a wide range of confining pressure (Liu et al., 2018a; Corti et al., 2017).

The generation of a stronger soil fabric is linked to the soil contractive behaviour (mainly during the virgin loading condition) and it is modelled through an expansion of the memory surface size. Contrarily, when the stress ratio is sufficiently high (i.e. when the stress path overcomes the phase transformation line PTL), damage of the soil fabric occurs trigging a partial loss of soil stiffness. This is phenomenologically represented by the a shrinkage of the memory surface. The evolution of the memory surface (i.e. change of the memory surface size m^M and the translation of the memory surface center $\boldsymbol{\alpha}^M$) cannot be independent. Therefore, the evolution of the memory surface size is expressed as follows in Liu et al. (2018a):

$$dm^M = dm_+^M - dm_-^M = \sqrt{\frac{3}{2}} d\boldsymbol{\alpha}^M : \boldsymbol{n} - \frac{m^M}{\zeta} f_{shr} \langle -d\varepsilon_v^p \rangle \tag{2}$$

where the first term on the right-hand side determines the expansion of the memory surface, while the second terms models the damage of soil fabric that occurs upon dilation - as suggested by Yimsiri and Soga (2010); Ziotopoulou and Boulanger (2016). The rate of damage is governed by the model constant ζ and by the term f_{shr} - see details in Appendix I of Liu et al. (2018a). However, for large strain levels, the soil behaviour is mainly governed by the relative soil density rather than generated soil fabric. This observation is incorporated into the model through a modified memory surface damage law:

$$dm^M = dm_+^M - dm_-^M = \sqrt{\frac{3}{2}} d\boldsymbol{\alpha}^M : \boldsymbol{n} - \frac{m^M}{\zeta} f_{shr} \langle -d\varepsilon_v^p \rangle F_{com} \langle b_r^b \rangle \tag{3}$$

where the term $F_{com}(t) = \int_0^t dm_+^M$ represents a factor accounting for the total "fabric generation" over the whole loading history up to current time. In the post-dilation regime, the rate of shrinkage of the memory surface is enhanced by larger values of F_{com}. It can be shown that large values of F_{com} are associated with large time of the soil spent in its "virgin state", i.e. with tangent memory and yield surfaces. As such, the hardening parameter h in Equation 1 degrades to $b_0/(\boldsymbol{r} - \boldsymbol{r}_{in}) : \boldsymbol{n}$ (i.e. without memory surface impact). The term $\langle b_r^b \rangle = \langle (\boldsymbol{r}^b - \boldsymbol{r}) : \boldsymbol{n} \rangle$ is introduced to avoid the conflict on the changing of the memory surface size during strain softening stage.

The translation rule for the memory surface center is as in the original publication:

$$d\boldsymbol{\alpha}^M = \frac{2}{3} \langle L \rangle h^M (\boldsymbol{r}^b - \boldsymbol{r}^M) \tag{4}$$

The dilatancy $D = A_d d$, where $d = (\boldsymbol{r}^d - \boldsymbol{r}) : \boldsymbol{n}$, with $\boldsymbol{r}^d$ the image point of $\boldsymbol{r}$ on the dilatancy surface. In order to adequately reproduce cyclic mobility responses (accumulation of shear strain in both positive and negative side of stress-strain plot under undrained symmetric cyclic loading condition), the dilatancy rule is modified as follows:

- for contracting ($d \geq 0$) following a contractive stage ($\tilde{b}_d^M \leq 0$), $A_d = A_0$ (where $\tilde{b}_d^M = (\tilde{\boldsymbol{r}}_\theta^d - \tilde{\boldsymbol{r}}^M) : \boldsymbol{n}$ tracks the position of the stress state with respect of the dilatancy surface)
- for contracting ($d \geq 0$) following a dilative stage ($\tilde{b}_d^M > 0$)

$$A_d = A_0 \exp \left[\beta_1 F \left(\frac{p}{p_N^{max}} \right)^{0.5} \right] g(\theta) \tag{5}$$

- for dilating ($d < 0$)

$$A_d = A_0 \exp \left[\beta_2 F \left(1 - \left(\frac{p}{p_N^{max}} \right)^{0.5} \right) \frac{d}{r_c} \right] \frac{1}{g(\theta)} \tag{6}$$

where A_0 is a model constant, p_N^{max} the maximum confining pressure up to current state. $F = \int_0^t dm_+^M + \int_0^t dm_-^M = F_{com} + F_{dilat}$ indicates the total fabric change. With $\boldsymbol{r}^c$ the image point of $\boldsymbol{r}$ on the critical surface, $r_c = \|\boldsymbol{r}^c\|$. β_1 and β_2 are the two dilatancy-related parameters. For the definition of the corresponding stress variables see Figure 1b.

3 MODEL CALIBRATION

Overall, the model contains 17 parameters (one additional parameter if compared to the original memory surface model by Liu et al. (2018a)) that can be divided into two sets: (1) the monotonic set of 13 parameters, from G_0 to n^d in Table 1, which can be calibrated from drained and/or undrained monotonic triaxial tests (Dafalias and Manzari, 2004; Liu et al., 2018a); (2) the four memory surface related parameters, i.e. from μ_0 to β_2 in Table 1, which can be calibrated from cyclic tests results such as drained/undrained cyclic triaxial tests.

Table 1. Model parameters for the quartz sand tested by Wichtmann (2005)

Elasticity		Critical state					Yield	Plastic modulus			Dilatancy		Memory surface			
G_0	ν	M	c	λ_c	e_0	ξ	m	h_0	c_h	n^b	A_0	n^d	μ_0	ζ	β_1	β_2
110	0.05	1.27	0.712	0.049	0.845	0.27	0.01	5.95	1.01	2.0	1.06	1.17	260	0.0001	1.9	2.4

The cyclic parameter μ_0 controls the ratcheting behaviour of sand under drained cases. For undrained conditions, it determines the amount of the generated pore water pressure during each cycle before dilation. For its calibration, either drained or undrained cyclic triaxial test can be selected. The damage parameter ζ is only relevant to stress paths beyond the PTL. Therefore, cyclic tests on dense sand with relatively high shear stress ratio or undrained cyclic triaxial tests are required for its calibration. In Table 1, the model parameters from G_0 to μ_0 have been calibrated by Liu et al. (2018a,b) for a quartz sand tested by Wichtmann (2005). The same values of them are adopted in this work to validate model performance under undrained cyclic loading conditions, since the same sand has been selected. Different from the value in Liu et al. (2018a), $\zeta = 0.0001$ is calibrated against the stress-strain relationship of undrained cyclic triaxial tests. The change will slightly affect the simulation result of Liu et al. (2018a) at large stress obliquity $\eta = q/p$. Dilatancy-related parameters β_1 and β_2 control the pore water pressure accumulation and the corresponding shear strain accumulation. Larger β_1 and/or smaller ζ result in larger reduction in effective stress p in post-dilation contraction; larger β_2 allows for larger post-dilation axial-strain accumulation. In this work $\beta_1 = 1.9$ and $\beta_2 = 2.4$ are calibrated through trial-and-error against undrained cyclic triaxial tests of Wichtmann (2005) on the same quartz sand, from shear stress-axial strain and $q - p$ relationship, respectively.

4 MODEL PERFORMANCE

Although the main purpose of the paper is to study the performance of the memory-surface model in simulating the undrained cyclic behaviour of sand, example of model performance under drained cyclic loading are reported for the sake of completeness and to show the full capabilities of this new model. The parameters in Table 1 are adopted for all simulations in the following. Explicit 4th order Runge-Kutta integration method is adopted for simulation.

4.1 *Drained cyclic test*

The drained high-cyclic model performance is validated by comparingc experimental with the simulation results regarding to accumulated total strain ($\varepsilon^{acc} = \sqrt{(\varepsilon_r^{acc})^2 + 2(\varepsilon_r^{acc})^2}$) against number of loading cycles N. As shown in Figure 2, the model predicts quite well the trends of accumulated strain with N up to 10^4 for varying average stress amplitudes q^{ampl}.

4.2 *Undrained cyclic test*

4.2.1 *Undrained cyclic DSS test*

Due to the lack of experimental data from undrained cyclic DSS test on the same sand type, the simulation results from the current model are only compared with the simulation results from the original model (Liu et al., 2018a). Figure 3a demonstrates that the original memory-surface model is unable to reproduce the proper cyclic stress-strain loop. The accumulation of shear strain γ ends after a few loading cycles (in this case, 4 cycles) on both the positive and the negative side, at a low strain level ($\gamma_{max} \approx \pm 0.01$). The new model successfully captures the progressive accumulation

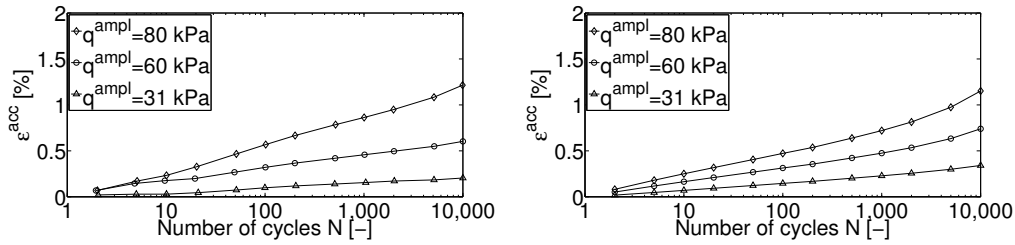

(a) Experimental results (Wichtmann, 2005) (b) Simulation from the current model

Figure 2.: Simulation results of drained cyclic triaxial tests: initial void ratio e_{in} =0.684, initial confining pressure p_{in} =200 kPa, average shear obliquity η^{ave} =0.75, number of cycles $N = 10^4$.

feature of the shear strain on both sides (see Figure 3b) during the post-dilation phase. In Figure 3b, the accumulated shear strain $\gamma_{max} \approx \pm 0.06$, which may vary depending on β_2.

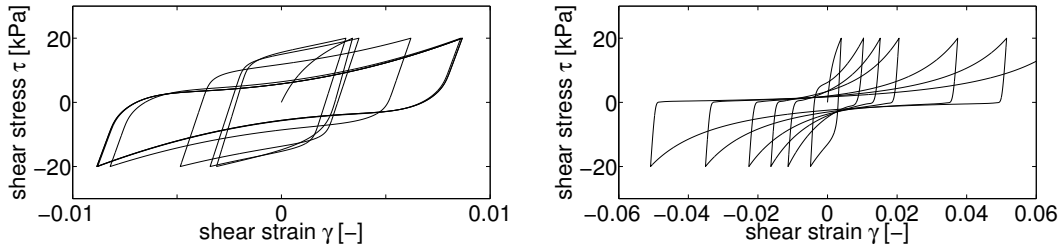

(a) Simulation from the original model (Liu et al., 2018a) (b) Simulation from the current model

Figure 3.: Simulation results of undrained cyclic DSS test: initial void ratio e_{in} =0.684, vertical stress σ_v =100 kPa, shear stress amplitude γ^{ampl} =20 kPa.

4.2.2 *Undrained cyclic triaxial tests*

In this part, the model's performance is studied in terms of simulating undrained cyclic triaxial tests with and without drained cyclic preloading. The modification on the shape of stress-strain loop of cyclic mobility is also presented.

Figure 4 shows the comparison between the experimental and the simulation results of undrained cyclic triaxial tests without drained cyclic pre-shear. The experimental results (Figure 4a) suggest that initial liquefaction occurs after 4 undrained loading cycles. Before initial liquefaction, almost no vertical strain is accumulated. The model predicts the initial liquefaction after only two cycles. This discrepancy can be erased if larger μ_0 value is adopted. Nevertheless, μ_0 =260 from Liu et al. (2018a) is still adopted, in order to balance the model performance on simulating both drained and undrained cyclic behaviour. Beyond this limited inaccuracy, it is worth noticing that the model predicts accumulation of the axial strain on both positive and negative sides, which agrees better with experimental observations in cyclic mobility phase. Moreover, comparable accumulated strain level is achieved (Figure 4b) - with the compression/extension asymmetry typically observed in triaxial tests.

The effect of cyclic preloading on the soil liquefaction resistance (defined as the number of undrained loading cycles required to cause initial liquefaction for given initial and loading conditions), which has been studied in the past decades (Finn et al., 1970; Seed et al., 1977; Suzuki and Toki, 1984; Seed et al., 1988; Teachavorasinskun et al., 1994), still remains an important aspect of soil behaviour where current understanding can be improved. To this end, in this work, the effect of drained cyclic preloading is explored and discussed using the proposed model.

In the work of Wichtmann (2005), drained cyclic loading was applied prior to the undrained cycles in cyclic triaxial tests on the quartz sand simulated. Model simulations of the same tests have been conducted and the comparison results are provided in Figure 5 and 6. The experimental results (compare Figure 5a and 6a with Figure 4a) suggest that drained cyclic preloading may increase soil liquefaction resistance, as long as the preshearing amplitudes are not too large

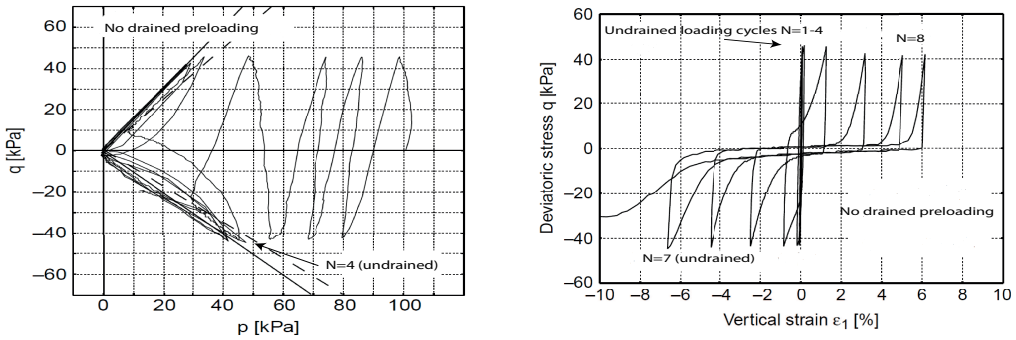

(a) Experimental results modified after Wichtmann (2005)

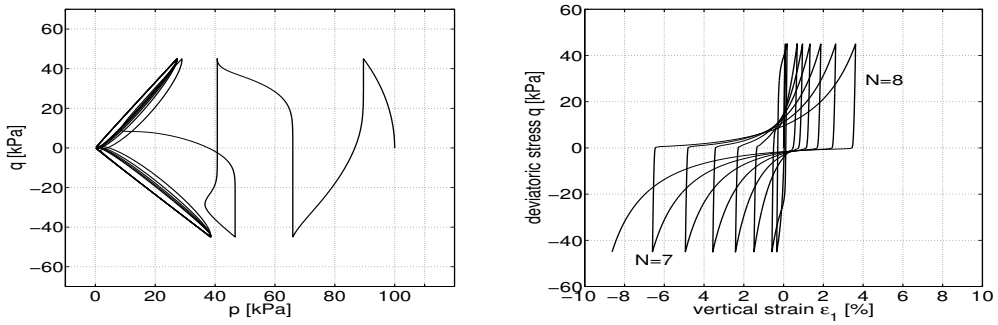

(b) Simulation results

Figure 4.: Comparison between (a) experimental (Wichtmann, 2005) and (b) simulation results: initial effective stress p_{in} =100 kPa, initial void ratio e_{in} =0.684, cyclic stress amplitude q^{ampl} =45 kPa, N = 8.

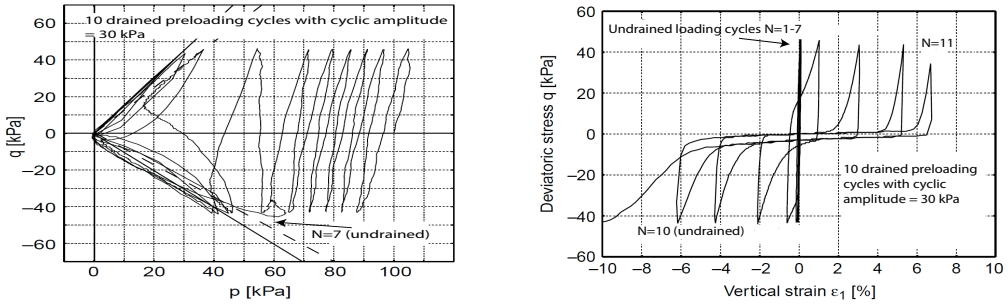

(a) Experimental results modified after Wichtmann (2005)

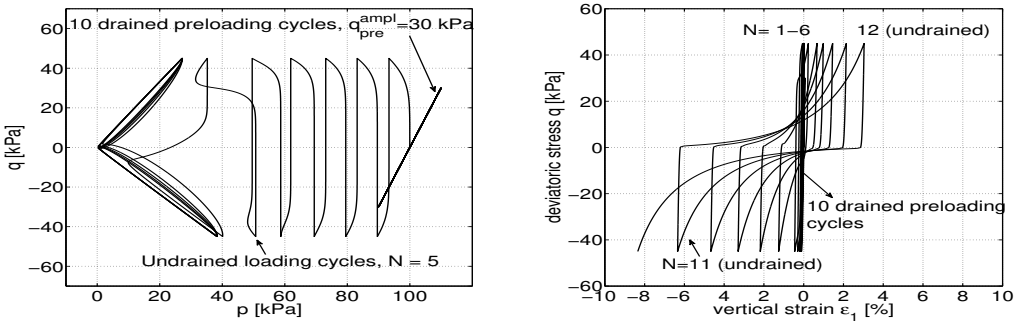

(b) Simulation results

Figure 5.: Comparison between (a) experimental (Wichtmann, 2005) and (b) simulation results: initial effective stress p_{in} =100 kPa, initial void ratio e_{in} =0.681, 10 undrained cycles (stress amplitude q^{ampl} =45 kPa) after 10 drained preloading cycles (stress amplitude q_{pre}^{ampl} =30 kPa).

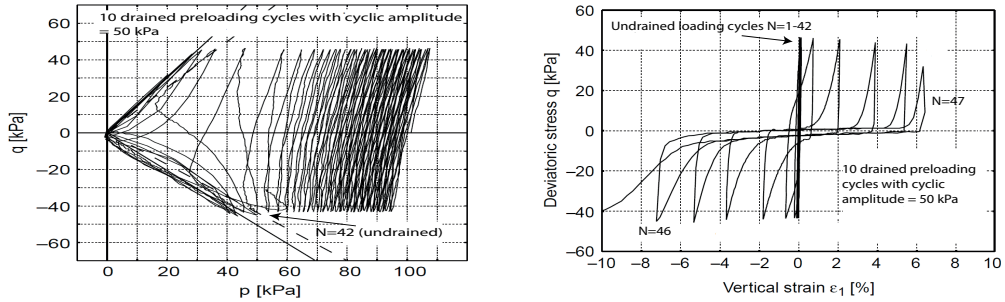

(a) Experimental results modified after Wichtmann (2005)

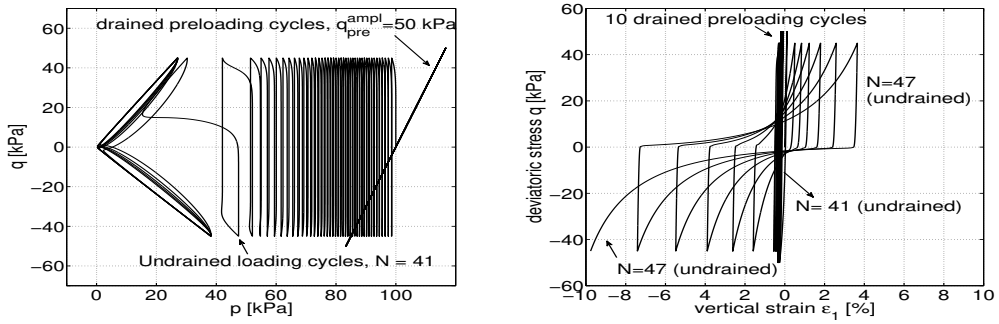

(b) Simulation results

Figure 6.: Comparison between (a) experimental (Wichtmann, 2005) and (b) simulation results: initial effective stress p_{in} =100 kPa, initial void ratio e_{in} =0.678, 54 undrained cycles (stress amplitude q^{ampl} =45 kPa) after 10 drained preloading cycles (stress amplitude q_{pre}^{ampl} =50 kPa).

(Suzuki and Toki, 1984; Wichtmann, 2005) (in these works, preloading stress paths are restricted to below PTL). For the same drained preloading cycles ($N = 10$ in Wichtmann's work), the larger preloading amplitude q_{pre}^{ampl} results in greater increase in soil cyclic undrained strength. In detail, for the case of $q_{pre}^{ampl} = 50$ kPa, soil sample experiences 42 undrained loading cycles before the initial liquefaction occurs. While for $q_{pre}^{ampl} = 30$ kPa, initial liquefaction happens after 8 undrained loading cycles (much earlier than $N = 42$ in the previous case, but still larger than $N = 4$ – case without drained cyclic preloading). Vertical strain mainly accumulates in the cyclic mobility stage on both compressive and extensive sides.

The increase in soil liquefaction resistance, which is linked to the generation of soil fabric during drained preloding cycles, is successfully captured by the model simulations (compare Figure 5b and 6b with Figure 4b) through the memory-enhanced hardening rule. The initial liquefaction is triggered after $N = 41$ (for the case of $q_{pre}^{ampl} = 50$ kPa) and $N = 5$ (for $q_{pre}^{ampl} = 30$ kPa) undrained loading cycles, both larger than $N = 2$ for non-preloading case. The model is able to predict the pore water pressure changes at the given number of loading cycles. Give the credit to the modified flow rule, the stress-strain loops in the cyclic mobility are appear much more realistic than predicted by the previous version of the model, although certainly improvable–see predicted accumulated vertical strain on the positive side.

5 CONCLUSION

An enhanced memory-surface hardening model was proposed by modifying the dilatancy relationship and incorporating a new memory-surface shrinkage law into the original model (Liu et al., 2018a). The model predictions agreed well with both undrained cyclic DSS and triaxial test results in terms of stress-strain loop in cyclic mobility stage and pore pressure generation under given loading cycles. The model can accurately predict ratcheting-related effects in both drained and undrained high-cyclic loading conditions. The model successfully captures the increasing of soil liquefaction resistance in presence of previous drained cyclic preloading. Overall, the model has high potential to predict reliable soil seismic behaviour in numerical simulations.

References

Andersen, K. H., 2009. Bearing capacity under cyclic loadingoffshore, along the coast, and on land. the 21st bjerrum lecture presented in oslo, 23 november 2007. Canadian Geotechnical Journal 46 (5), 513–535.

Been, K., Jefferies, M. G., 1985. A state parameter for sands. Géotechnique 35 (2), 99–112.

Corti, R., Diambra, A., Wood, D. M., Escribano, D. E., Nash, D. F., 2016. Memory surface hardening model for granular soils under repeated loading conditions. Journal of Engineering Mechanics 142 (12), 04016102.

Corti, R., Gourvenec, S. M., Randolph, M. F., Diambra, A., 2017. Application of a memory surface model to predict whole-life settlements of a sliding foundation. Computers and Geotechnics 88, 152–163.

Dafalias, Y. F., Manzari, M. T., 2004. Simple plasticity sand model accounting for fabric change effects. Journal of Engineering mechanics 130 (6), 622–634.

Elgamal, A., Yang, Z., Parra, E., Ragheb, A., 2003. Modeling of cyclic mobility in saturated cohesionless soils. International Journal of Plasticity 19 (6), 883–905.

Finn, W., Bransby, P. L., Pickering, D. J., 1970. Effect of strain history on liquefaction of sand. Journal of Soil Mechanics & Foundations Div 96 (SM6).

Ishihara, K., 1993. Liquefaction and flow failure during earthquakes. Géotechnique 43 (3), 351–451.

Liu, H. Y., Abell, J. A., Diambra, A., Pisanò, F., 2018a. Modelling the cyclic ratcheting of sands through memory-enhanced bounding surface plasticity. Géotechnique, 1–18.

Liu, H. Y., Pisanò, F., 2018. Prediction of oedometer terminal densities through a memory-enhanced plasticity model for sand. Géotechnique letters accepted for publication.

Liu, H. Y., Zygounas, F., Diambra, A., Pisanò, F., 2018b. Enhanced plasticity modelling of high-cyclic ratcheting and pore pressure accumulation in sands. In: Numerical Methods in Geotechnical Engineering IX, Volume 1: Proceedings of the 9th European Conference on Numerical Methods in Geotechnical Engineering (NUMGE 2018), June 25-27, 2018, Porto, Portugal. CRC Press, pp. 87–95.

Seed, H. B., Mori, K., Chan, C., 1977. Influence of seismic history on liquefaction of sands. Journal of Geotechnical and Geoenvironmental Engineering 103 (Proc. Paper 11318 Proceeding).

Seed, R. B., Lee, S. R., Jong, H.-L., 1988. Penetration and liquefaction resistances: Prior seismic history effects. Journal of Geotechnical Engineering 114 (6), 691–697.

Suzuki, T., Toki, S., 1984. Effects of preshearing on liquefaction characteristics of saturated sand subjected to cyclic loading. Soils and Foundations 24 (2), 16–28.

Teachavorasinskun, S., Tatsuoka, F., Lo Presti, D. C. F., 1994. Effects of the cyclic prestraining on dilatancy characteristics and liquefaction strength of sand. In: IS HOKKAIDO 94. Vol. 1. AA Balkema, pp. 75–80.

Wichtmann, T., 2005. Explicit accumulation model for non-cohesive soils under cyclic loading. Ph.D. thesis, Inst. für Grundbau und Bodenmechanik Bochum University, Germany.

Yang, J., Sze, H., 2011. Cyclic behaviour and resistance of saturated sand under non-symmetrical loading conditions. Géotechnique.

Yimsiri, S., Soga, K., 2010. Dem analysis of soil fabric effects on behaviour of sand. Géotechnique 60 (6), 483.

Ziotopoulou, K., Boulanger, R., 2013. Calibration and implementation of a sand plasticity plane-strain model for earthquake engineering applications. Soil Dynamics and Earthquake Engineering 53, 268–280.

Ziotopoulou, K., Boulanger, R., 2016. Plasticity modeling of liquefaction effects under sloping ground and irregular cyclic loading conditions. Soil Dynamics and Earthquake Engineering 84, 269–283.